Comparison between length and velocity gauges in quantum simulations of high-order harmonic generation

Yong-Chang Han and Lars Bojer Madsen

Lundbeck Foundation Theoretical Center for Quantum System Research, Department of Physics and Astronomy,
Aarhus University, DK-8000 Aarhus C, Denmark

We solve the time-dependent Schrödinger equation for atomic hydrogen in an intense field using spherical coordinates with a radial grid and a spherical harmonic basis for the angular part. We present the high-order harmonic spectra based on three different forms, the dipole, dipole velocity, and acceleration forms, and two gauges, the length and velocity gauges. The relationships among the harmonic phases obtained from the Fourier transform of the three forms are discussed in detail. Although quantum mechanics is gauge invariant and the length and velocity gauges should give identical results, the two gauges present different computation efficiencies, which reflects the different behavior in terms of characteristics of the physical couplings acting in the two gauges. In order to obtain convergence, more angular momentum states are required in the length gauge, while more grid points are required in the velocity gauge. At lower laser intensity, the calculation in the length gauge is faster than that in the velocity gauge, while at high laser intensity, the calculation in the velocity gauge is more efficient. The velocity gauge is also expected to be more efficient in higher-dimensional calculations.

I. INTRODUCTION

When an atom or molecule interacts with an intense femtosecond laser pulse, an electron may escape into the continuum, where it propagates in the field, and when the oscillating field changes its direction the electron may be steered back to the parent ion and possibly recombine with the emission of high-frequency coherent radiation [1]. This high-order harmonic generation (HHG) process has attracted a lot of interest during the past couple of decades (for reviews, see, e.g., Refs. [2,3]). Apart from the obvious interest in coherent sources extending into the XUV regime, one can use HHG to generate attosecond pulses [4–7] and to obtain information about molecular structure and orbitals (see, e.g., Refs. [8–13]). The HHG spectrum corresponding to the response of a single quantum system can be calculated in three alternative forms: from the modulus square of the Fourier transform of the time-dependent expectation value of (i) the dipole moment $\boldsymbol{r}$, (ii) the dipole velocity $\dot{\boldsymbol{r}}$, or (iii) the dipole acceleration $\ddot{\boldsymbol{r}}$ [14]. In addition to these three forms, there are two commonly used gauges to describe the interaction between matter and the electromagnetic field: the length gauge (LG) and the velocity gauge (VG). Based on the two different gauges, one can solve the time-dependent Schrödinger equation (TDSE) to obtain the time-dependent wave function. For the calculation of the HHG spectrum, the three forms and two gauges, make in total six different combinations (see Sec. II). Since quantum mechanics is gauge invariant, the results obtained from the two gauges after the end of the induced electron motion should be the same, although results obtained with approximate theoretical models may be gauge dependent (see, e.g., Refs. [15–17]). Alternatively the vector potential in the VG formulation can be appropriately shifted [18]. Besides the TDSE method, there are also other theoretical methods that can be used to calculate the HHG spectrum. In the long-pulse limit, for example, Floquet theory combined with complex scaling can be used (see, e.g., Refs. [19–26]).

The formal theoretical identity of results obtained in the two gauges does not necessarily mean that such an identity can be obtained in practical numerical calculations. The two formulations may impose different demands on computations in terms of basis size and cost of CPU time. Such a situation was discussed in detail some years ago [27] in the context of above threshold ionization (ATI) and it was found that the VG was the optimal gauge. In that paper, the TDSE was solved in a box using a *B* splines basis for the radial part and spherical harmonics basis for the angular part. The box and the number and order of *B* splines were fixed and it was found that many more angular momenta were needed in order to obtain converged results for the ATI spectra in the LG, and in fact cases were presented where convergence could only be obtained in the VG. For HHG no systematical study of the differences between the two gauges has so far been presented in the literature, and it is the purpose of the present work to undertake such an investigation. Now, in the HHG case, the interest is of course on the spectra, but also on the phases of the expectation values of $\boldsymbol{r}$, $\dot{\boldsymbol{r}}$, and $\ddot{\boldsymbol{r}}$. These phases are needed, for example, to be able to determine the polarization properties of the generated high-order harmonic radiation [28–30]. As we show, different demands on the radial discretization of the problem are imposed in the LG and the VG, respectively, to obtain convergence of these phases.

Performing full-dimensional TDSE quantum calculations of a single quantum system's response with the aim of studying HHG is computationally heavy [31–36]. Recently, the three forms for calculating the HHG spectra taking the hydrogen atom as an example were investigated by performing the propagation of the TDSE in the LG [14]. In that study, the three different forms were compared for different laser intensities and carrier envelope phases and the relationship among the spectra in the three alternative forms was discussed [see Eq. (3)]. In this work we perform calculations in both the LG and the VG for the hydrogen atom. We point out that the dipole velocity follows different forms in the LG

and the VG, respectively, while the forms of dipole and dipole acceleration are identical in the two gauges. We also demonstrate that the simplified formula which can be used to explain the relationship of the spectrum intensities of the three forms cannot be extended to explain the relationship among their phases. We obtain identical results in the two gauges, and the results agree with the LG results of Ref. [14], providing a further proof of the convergence and making the present set of results very useful for benchmarking numerical calculations of HHG. We find that the calculations based on the two gauges have different efficiencies depending on the intensity of the external field, and we rationalize the different behavior in terms of characteristics of the physical couplings acting in the two gauges. Our study is also motivated by the current interest [37–39] in the use of the TDSE to generate the dipole of the single-system response and from that determine the macroscopic polarization of a medium subject to a strong pulse. The polarization then enters Maxwell's wave equation as a source term and generation and propagation of HHG radiation can be described by a combined TDSE-Maxwell wave equation approach. Clearly, such an approach requires huge computational resources and it is important to be able to solve the TDSE quickly and efficiently for a practical implementation, and also in this connection the question about optimal gauge and relations between results obtained in different gauges becomes of relevance.

II. THEORY

The HHG spectrum from an atom can be obtained from the Fourier transform of the time-dependent expectation values of the dipole, dipole velocity, and dipole acceleration, $\boldsymbol{\zeta} = \{\boldsymbol{r}, \dot{\boldsymbol{r}}, \ddot{\boldsymbol{r}}\}$ [14]. The spectrum along the direction of the unit vector $\hat{\boldsymbol{e}}$ is given by (see, e.g., [40])

$$S^{\hat{e}}_{\zeta}(\omega) \sim \left| \int_0^{t_f} \hat{\boldsymbol{e}} \cdot \langle \boldsymbol{\zeta}(t) \rangle e^{-i\omega t} dt \right|^2$$
$$= \left| \int_0^{t_f} \hat{\boldsymbol{e}} \cdot \langle \Psi(t) | \boldsymbol{\zeta} | \Psi(t) \rangle e^{-i\omega t} dt \right|^2. \quad (1)$$

Depending on the excitation dynamics, t_f is the pulse duration, with $t_f = T$ or longer; we return to this point shortly. By invoking the symmetry-dictated condition $\langle \boldsymbol{\zeta}(t_i = 0) \rangle = 0$ for the atomic case studied here, the Fourier transform of the three forms can be related to each other by partial integration,

$$\int_0^{t_f} \langle \dot{\boldsymbol{r}} \rangle e^{-i\omega t} dt = \langle \boldsymbol{r} \rangle |_{t_f} e^{-i\omega t_f} + i\omega \int_0^{t_f} \langle \boldsymbol{r} \rangle e^{-i\omega t} dt,$$
$$\int_0^{t_f} \langle \ddot{\boldsymbol{r}} \rangle e^{-i\omega t} dt = \langle \dot{\boldsymbol{r}} \rangle |_{t_f} e^{-i\omega t_f} + i\omega \int_0^{t_f} \langle \dot{\boldsymbol{r}} \rangle e^{-i\omega t} dt. \quad (2)$$

Thus, if the expectation values of the dipole and dipole velocity at the final time ($t_f = T$) satisfy $\langle \boldsymbol{r}(t_f) \rangle \approx \langle \dot{\boldsymbol{r}}(t_f) \rangle \approx 0$, the spectra can be simply related by the expression [14]

$$\omega^4 S^{\hat{e}}_r(\omega) \approx \omega^2 S^{\hat{e}}_{\dot{r}}(\omega) \approx S^{\hat{e}}_{\ddot{r}}(\omega). \quad (3)$$

This condition is typically satisfied in a relatively weak laser field where not much population is left in excited states after the end of the pulse. At higher intensity where the excited states are populated to a higher extent at the end of the pulse, $\langle \boldsymbol{r}(t = T) \rangle$

and $\langle \dot{\boldsymbol{r}}(t = T) \rangle$ will be significantly different from zero. To account for the decay of the dipole in this case, spontaneous radiative decay rates for the excited states could in principle be included and the integration limit extended to times $t_f \gg T$ on the nanosecond time scale where then $\langle \boldsymbol{r}(t_f) \rangle \approx \langle \dot{\boldsymbol{r}}(t_f) \rangle \approx 0$, and the simple relationship still works. In practical calculations the propagation to such long time scales would imply very long integration times, and it is customary to restrict the integration interval to $t_f = T$ and we shall do so in the following.

The phase of a given harmonic in single-system TDSE calculations is estimated from the phase of the Fourier transform of the dipole. The phases pertaining to the three forms are related as described in Eq. (2) and are sensitive to the first terms on the right-hand side of Eq. (2).

We note that if a molecular target is considered, Eq. (1), giving the HHG spectrum, should be changed according to the discussion in Refs. [11,41] to take into account the alignment and orientation distribution with respect to the external field axis.

In order to obtain the spectrum, one needs to calculate the time-dependent wave function. The TDSE for the full wave function can be expressed as

$$i\frac{\partial}{\partial t}\Psi(\boldsymbol{r},t) = \left(-\frac{\boldsymbol{\nabla}^2}{2} - \frac{1}{r} + W(\boldsymbol{r},t) \right) \Psi(\boldsymbol{r},t) \quad (4)$$

(where atomic units are used throughout unless indicated otherwise), with the laser-matter interaction term defined as

$$W(\boldsymbol{r},t) = \begin{cases} \boldsymbol{r} \cdot \boldsymbol{E}(t) & \text{(LG)}, \\ -i\boldsymbol{A}(t) \cdot \boldsymbol{\nabla} & \text{(VG)}. \end{cases} \quad (5)$$

Here $\boldsymbol{E}(t) = -\partial_t \boldsymbol{A}(t)$ is the electric field and $\boldsymbol{A}(t)$ is the corresponding vector potential. We note that the VG used in this work is sometimes refereed to as the reduced VG [42]; that is, the laser-matter interaction term of the VG in Eq. (5) does not include the time-dependent potential $A^2(t)/2$, which is spatially independent and hence does not affect the expectation values of dipole, dipole velocity, and dipole acceleration. From Eq. (4) we obtain the Schrödinger equation for the reduced wave function $\psi(\boldsymbol{r},t) = r\Psi(\boldsymbol{r},t)$:

$$i\frac{\partial}{\partial t}\psi(\boldsymbol{r},t) = \left(-\frac{1}{2}\frac{\partial^2}{\partial r^2} + \frac{L^2}{2r^2} - \frac{1}{r} + W_r(\boldsymbol{r},t) \right) \psi(\boldsymbol{r},t), \quad (6)$$

with

$$L^2 = -\frac{1}{\sin\theta}\frac{\partial}{\partial\theta}\left(\sin\theta\frac{\partial}{\partial\theta} \right) - \frac{1}{\sin^2\theta}\frac{\partial^2}{\partial\phi^2} \quad (7)$$

and

$$W_r(\boldsymbol{r},t) = \begin{cases} \boldsymbol{r} \cdot \boldsymbol{E}(t) & \text{(LG)}, \\ -i\boldsymbol{A}(t) \cdot (\boldsymbol{\nabla} - \hat{\boldsymbol{r}}/r) & \text{(VG)}. \end{cases} \quad (8)$$

In order to solve Eq. (6), we expand the reduced wave function $\psi(\boldsymbol{r},t)$ in a series of spherical harmonics for the angular part with unknown reduced radial functions $f_{lm}(r,t)$:

$$\psi(r,\theta,\phi,t) = \sum_{l=0}^{L_{\max}} \sum_{m=-l}^{l} f_{lm}(r,t) Y_{lm}(\theta,\phi). \quad (9)$$

In the case of the H atom interacting with a linearly polarized laser pulse, the azimuthal quantum number m is a constant due

to the cylindrical symmetry and is initially set to be 0, since we start out in the $1s$ ground state.

The TDSE is solved numerically using grid methods [43,44]. We obtain the time-dependent wave function in both the LG and the VG, denoted by $\Psi_{\mathrm{LG}}(\boldsymbol{r},t)$ and $\Psi_{\mathrm{VG}}(\boldsymbol{r},t)$, respectively. As is well known, there are transformations from one gauge to the other for the wave functions [42,45–47]

$$\Psi_{\mathrm{LG}}(\boldsymbol{r},t) = e^{iA\cdot r}\Psi_{\mathrm{VG}}(\boldsymbol{r},t) \qquad (10)$$

and for the operators

$$\hat{O}_{\mathrm{VG}} = e^{-iA\cdot r}\hat{O}_{\mathrm{LG}}\,e^{iA\cdot r}. \qquad (11)$$

Based on these relationships, the expectation value of an operator fulfills

$$\langle\hat{O}_{\mathrm{VG}}\rangle_{\mathrm{VG}} = \langle e^{-iA\cdot r}\hat{O}_{\mathrm{LG}}\,e^{iA\cdot r}\rangle_{\mathrm{VG}} = \langle\hat{O}_{\mathrm{LG}}\rangle_{\mathrm{LG}}. \qquad (12)$$

From Eq. (11), we see that if $[\hat{O}_{\mathrm{LG}},e^{iA\cdot r}]=0$, the operator will have the same form in the LG and the VG. This case takes place when we calculate the expectation values of the dipole and dipole acceleration. We assume that the laser polarization direction is along the z axis [i.e., in Eq. (1), $\hat{\boldsymbol{e}}\cdot\boldsymbol{\zeta}=z,\dot{z},\ddot{z}$]. In the LG, the expectation values of the dipole and dipole acceleration (where we recall Ehrenfest's theorem) along the z axis can be expressed as

$$\langle z\rangle\,|_{\mathrm{LG}} = \langle\Psi_{\mathrm{LG}}(\boldsymbol{r},t)|\cos\theta\,r|\Psi_{\mathrm{LG}}(\boldsymbol{r},t)\rangle,$$
$$\langle\ddot{z}\rangle\,|_{\mathrm{LG}} = -\langle\Psi_{\mathrm{LG}}(\boldsymbol{r},t)|\partial_z V(\boldsymbol{r}) + E(t)|\Psi_{\mathrm{LG}}(\boldsymbol{r},t)\rangle \qquad (13)$$
$$= -\langle\Psi_{\mathrm{LG}}(\boldsymbol{r},t)|\frac{\cos\theta}{r^2} + E(t)|\Psi_{\mathrm{LG}}(\boldsymbol{r},t)\rangle.$$

Clearly the operators in Eq. (13) satisfy $[\cos\theta\,r,e^{iA\cdot r}]=0$ and $[\cos\theta\,r^{-2} + E(t),e^{iA\cdot r}]=0$. So the dipole and dipole acceleration operators are identical in the LG and the VG, and, accordingly,

$$\langle z\rangle\,|_{\mathrm{VG}} = \langle\Psi_{\mathrm{VG}}(\boldsymbol{r},t)|\cos\theta\,r|\Psi_{\mathrm{VG}}(\boldsymbol{r},t)\rangle,$$
$$\langle\ddot{z}\rangle\,|_{\mathrm{VG}} = -\langle\Psi_{\mathrm{VG}}(\boldsymbol{r},t)|\partial_z V(\boldsymbol{r}) + E(t)|\Psi_{\mathrm{VG}}(\boldsymbol{r},t)\rangle \qquad (14)$$
$$= -\langle\Psi_{\mathrm{VG}}(\boldsymbol{r},t)|\frac{\cos\theta}{r^2} + E(t)|\Psi_{\mathrm{VG}}(\boldsymbol{r},t)\rangle.$$

Nevertheless, if $[\hat{O}_{\mathrm{LG}},e^{iA\cdot r}]\neq 0$, the operator will have different forms in the LG and the VG. This takes place when we calculate the dipole velocity in the two gauges. In the LG, the expectation value of the dipole velocity is expressed as

$$\langle\dot{z}\rangle\,|_{\mathrm{LG}} = \langle\Psi_{\mathrm{LG}}(\boldsymbol{r},t)|p_z|\Psi_{\mathrm{LG}}(\boldsymbol{r},t)\rangle, \qquad (15)$$

with $p_z = -i\partial_z$. However, in the VG, the formula changes to be

$$\langle\dot{z}\rangle\,|_{\mathrm{VG}} = \langle\Psi_{\mathrm{VG}}(\boldsymbol{r},t)|e^{-iA\cdot r}p_z\,e^{iA\cdot r}|\Psi_{\mathrm{VG}}(\boldsymbol{r},t)\rangle$$
$$= \langle\Psi_{\mathrm{VG}}(\boldsymbol{r},t)|p_z - iA[z,p_z]|\Psi_{\mathrm{VG}}(\boldsymbol{r},t)\rangle$$
$$= \langle\Psi_{\mathrm{VG}}(\boldsymbol{r},t)|p_z + A(t)|\Psi_{\mathrm{VG}}(\boldsymbol{r},t)\rangle. \qquad (16)$$

The result (16) could have been written up directly by remembering that $\boldsymbol{\pi} = \boldsymbol{p} + \boldsymbol{A}$ is the kinematical momentum in the VG. The result in (15) is unique in the sense that it is only in the LG that the canonical, $\boldsymbol{p}$, and kinematical, $\boldsymbol{\pi}$, momenta coincide.

III. RESULTS AND DISCUSSION

We calculate harmonic spectra using the three forms in both length and velocity gauges. We use a sine-square laser envelope and express the field and the vector potential as

$$\boldsymbol{E}(t) = E_0\left[\sin^2\left(\frac{\pi t}{T}\right)\sin(\omega_0 t)\right.$$
$$\left. - \frac{\pi}{\omega_0 T}\sin\left(\frac{2\pi t}{T}\right)\cos(\omega_0 t)\right]\hat{z}, \qquad (17)$$
$$\boldsymbol{A}(t) = \frac{E_0}{\omega_0}\sin^2\left(\frac{\pi t}{T}\right)\cos(\omega_0 t)\hat{z}.$$

We use a laser wavelength of 800 nm with an optical cycle time of 110.32 a.u.. The pulse duration T is set to be three optical cycles. The normalized electric field $E(t)$ and vector potential $A(t)$ are shown in Fig. 1.

The results in both length and velocity gauges are shown in Fig. 2 for a laser intensity of 0.3×10^{14} W/cm^2. The time-dependent expectation values of the dipole, dipole velocity, and dipole acceleration are shown in the left panels (a)–(c), and the corresponding harmonic spectra are shown to the right, (d)–(f). The solid (black) curves show the results obtained in the LG, while the dashed (red) curves show the results obtained in the VG. From Fig. 2 we see that the LG and the VG give the same results for the dipole, dipole velocity, and dipole acceleration. Also the spectra in the three forms exhibit very similar shapes. This is because the laser intensity is much lower than the threshold for over-the-barrier ionization ($I_b = 1.4\times 10^{14}$ W/cm^2). At such a low intensity, the expectation values of the dipole and dipole velocity at the end of the pulse ($t_f = T$), $\langle z(t_f)\rangle$, $\langle\dot{z}(t_f)\rangle$, are nearly equal to zero, as shown in Figs. 2(a) and 2(b). Thus, the spectra of the three forms will follow the simple relationship Eq. (3). Indeed if we scale the spectra with the appropriate factors of ω^2 and ω^4, they are all on top of each other. This result agrees with the findings reported in Ref. [14].

In order to obtain the correct expectation value of dipole velocity in the VG, Eq. (16) should be used, instead of just the expectation value of p_z [compared to the form Eq. (15) which works in the LG]. In Fig. 3, the expectation values of $p_z + A(t)$ and p_z in the VG are shown. It can be seen that the two curves are different from each other not only in
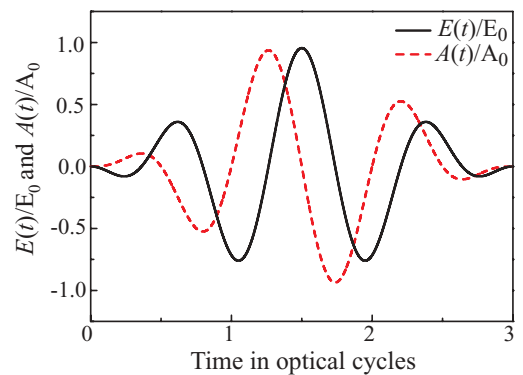

FIG. 1. (Color online) Normalized electric field $E(t)$ (solid black curve) and vector potential $A(t)$ (dashed red curve) of Eq. (17). The wavelength is 800 nm.
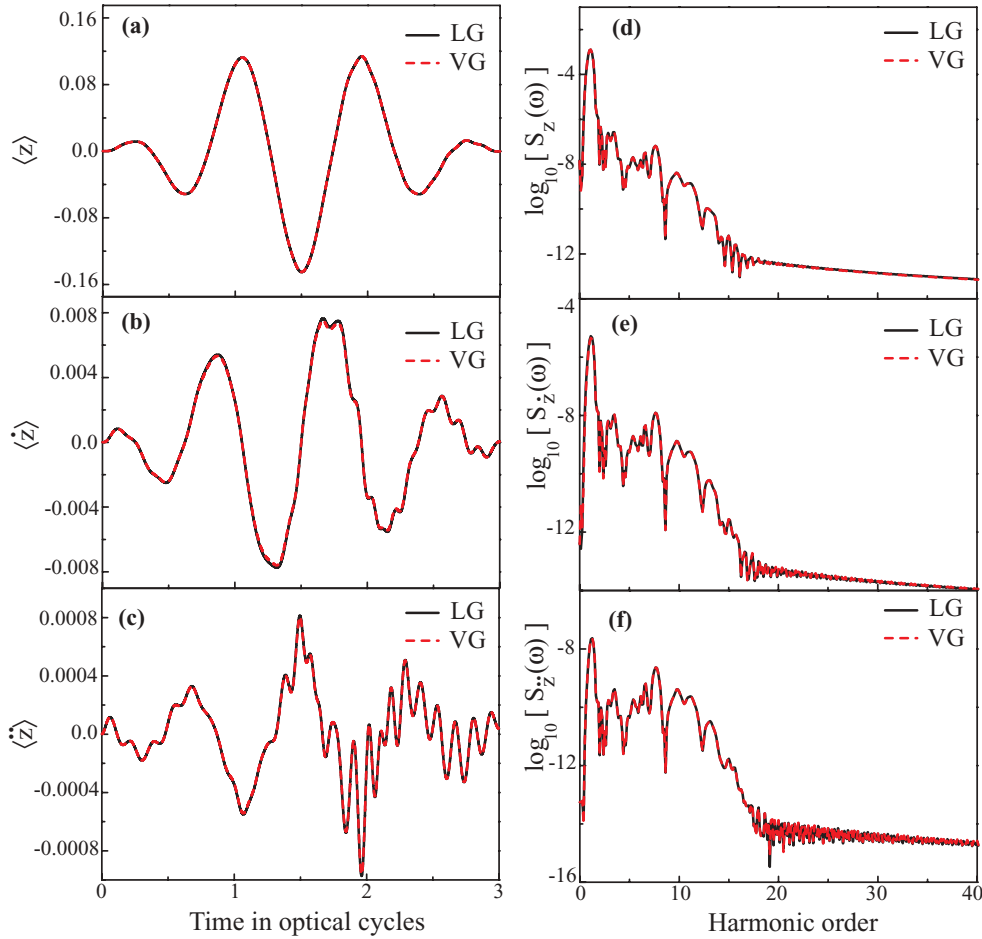
FIG. 2. (Color online) Expectation values in atomic units of the (a) dipole, (b) dipole velocity, and (c) a dipole acceleration, and the corresponding harmonic spectra (d)–(f) as a function of harmonic order, for a laser wavelength of 800 nm and an intensity of 0.3×10^{14} W/cm^2. The solid black and dashed red curves refer to the results in the length (LG) and velocity (VG) gauges, respectively.

the shapes but also in the scales, stressing the importance of working with the kinematical momenta $\boldsymbol{\pi}$ in the VG. It is easy to extend Eq. (16) to higher dimensional cases, where harmonic components along x, y come to play.
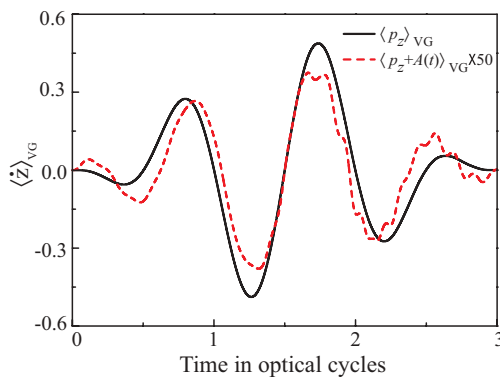

FIG. 3. (Color online) Expectation values in atomic units of p_z (solid black) and $p_z + A(t)$ (dashed red) in the velocity gauge, for a laser wavelength of 800 nm and an intensity of 0.3×10^{14} W/cm^2. Note the difference in the scale.

Although the calculation in both the LG and the VG can give the same results, we find that different kinds of parameters are needed to obtain convergence in the LG and the VG, respectively. In both cases the range of the radial grid is 125 bohr with an absorption boundary to avoid unphysical reflection from the continuum part of the electron density describing ionization. In the LG, we take $N_r = 1400$ and $L_{\max} = 15$ to describe the radial and angular parts of the wave function, respectively. In the VG, we need $N_r = 1500$ and only $L_{\max} = 9$ to obtain convergence. The results are repeated in a larger box with more grid points and larger $L_{\max}$ for both the LG and the VG. We find that more points of the radial grid are required in the VG than in the LG and that higher $L_{\max}$ is required in the LG than in the VG.

The difference in the scaling in $L_{\max}$ has been discussed before (see, e.g., [27,48]). In short the more favorable scaling in the VG can be understood by noting that the canonical momentum in the VG is reduced by the vector potential, whereas such a reduction is not present in the LG. The difference in canonical momentum induces the corresponding difference in the angular momentum, $\boldsymbol{L} = \boldsymbol{r} \times \boldsymbol{p}$. An alternative way of arguing is to imagine that the wave packet is represented in a basis of field-free eigenstates and to consider the difference
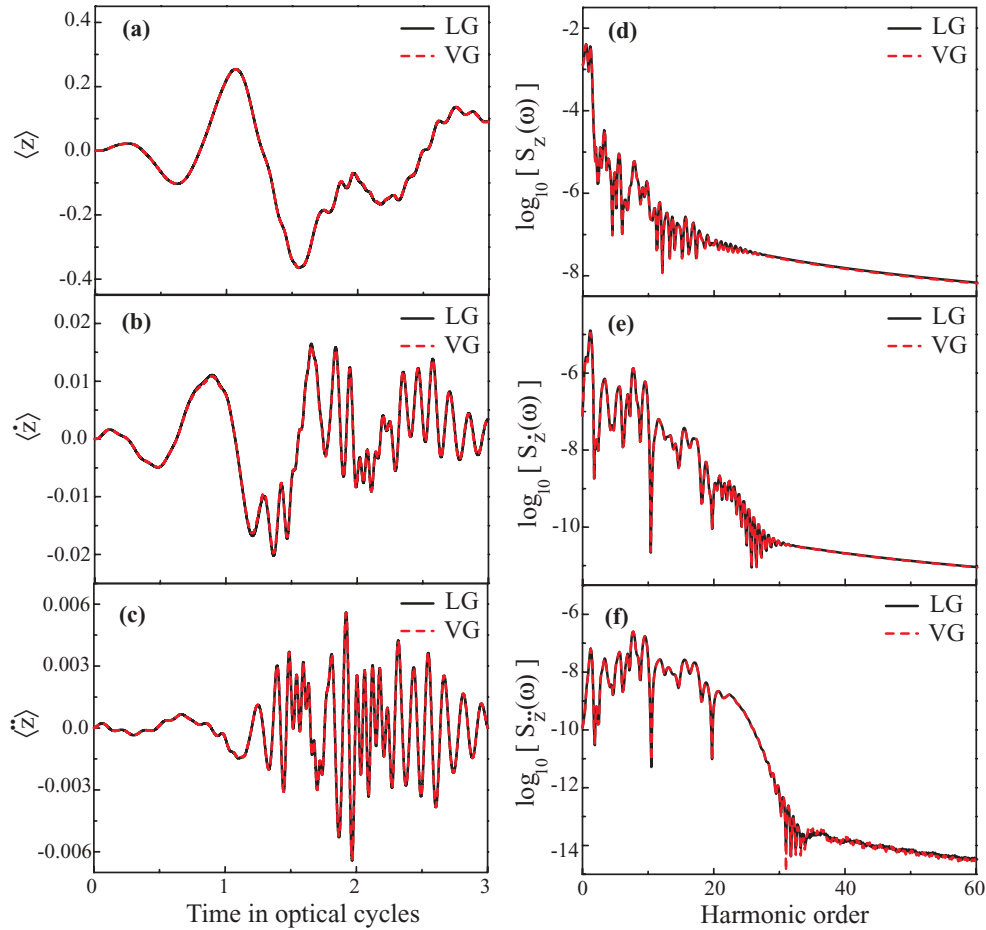
FIG. 4. (Color online) Same as Fig. 2, expect that the laser intensity has been increased to 1.138×10^{14} W/cm^2.

between the laser-induced couplings between the field-free states in the two gauges. In the LG, the dipole coupling tends to become very large between spatially extended excited states that are close in energy [49], leading to a rapid increase in the angular momentum. In the VG, on the other hand, we may express the canonical momentum by the commutator of the field-free Hamiltonian and the spatial coordinate, $\boldsymbol{p} = i[H_0, \boldsymbol{r}]$, which shows the such couplings in VG are suppressed by a factor accounting for the energy difference between the field-free states involved, effectively leading to less coupling to high-l states.

For the scaling with the number of grid points, the difference can be understood by noting that it takes more grid points to represent the interaction between the gradient operator ∇ and the radial part of the wave function than is the case in the LG, where no differentiation is involved. In the LG, regions of large r gain relatively more weight by the interaction than the smaller r region, and for large r the wave packet is relatively slowly varying. Oppositely in the VG, the differential operator weights spatial regions with fast changes in the wave packet (closer to the core). To sample such changes accurately more grid points are needed in the VG than in the LG. From this discussion we expect that the different behaviors of the two gauges will be very dependent on the laser intensity and independent of other laser parameters such as the pulse duration and the frequency (i.e., when the laser intensity is

high, many angular momenta are needed in the LG and many grid points are needed in the VG to characterize the part of the wave packet closer to the core).

To confirm these points quantitatively, we calculate the results at a higher intensity. In Fig. 4, we show the same physical quantities as in Fig. 2, but for the increased intensity of 1.138×10^{14} W/cm^2. The expectation values of the three forms are shown in the left panels, and the corresponding harmonic spectra are to the right. The solid (black) curves are results obtained in the LG, while the dashed (red) curves denote results obtained in the VG. The results obtained in the two gauges are still in good agreement with each other. Nevertheless, the spectra of the three forms are different from each other. There are small deviations above the cutoffs in regions with almost no signal, most clearly seen in (e) and (f), and these differences are due to numerical imperfections, which do not affect the spectra in the regions where there is some signal.

In such an intense laser field, with a field strength comparable to the threshold for over-the-barrier ionization, the expectation values of dipole and dipole velocity at the end of the pulse, $\langle z(t_f = T) \rangle$, $\langle \dot{z}(t_f = T) \rangle$, are very far from zero, as displayed in Figs. 3(a) and 3(b). Thus, the simple relationship of Eq. (3) among the spectra in the three forms breaks down [14]. What is more, in such an intense field, we have to take $N_r = 1600$ (1800) and $L_{max} = 35$ (15) to get
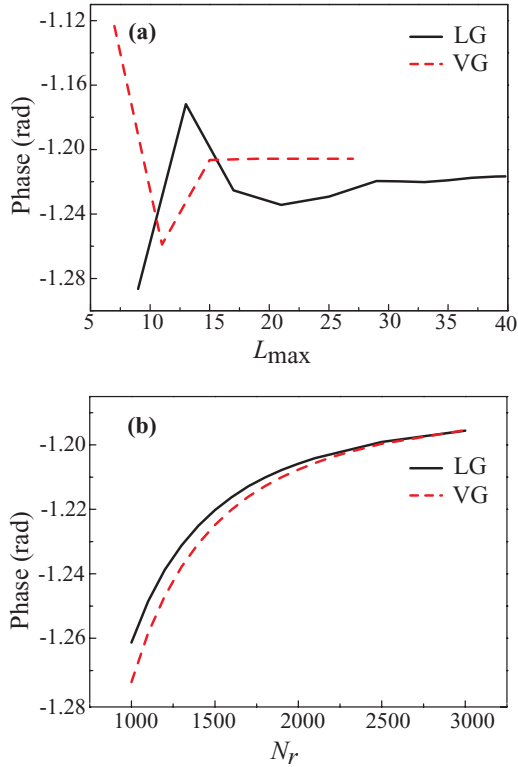
FIG. 5. (Color online) Phase of the fifth harmonic as obtained from the Fourier transform of the time-dependent dipole velocity for an intensity of 1.138×10^{14} W/cm^2 (a) as a function of L_{max} for $N_r = 1600$ (1800) in the LG (VG) and (b) as a function of N_r for $L_{max} = 35$ (15) in the LG (VG). Full (dashed) curves are LG (VG) results.

convergence in the LG (VG). The box range is the same as that used in Fig. 2. It can be seen that in both strong and weak fields, one needs more angular basis states, that is, more spherical harmonics in the LG than in the VG, and more grid points in the VG than in the LG, to obtain convergence. Moreover, due to the increase of laser intensity, L_{max} in the LG increases from 15 to 35, a more than 100% rise. At the same time, the number of grid points, N_r, in the VG increases only from 1500 to 1800, only a 20% increase. These results show that to calculate HHG for increasing intensity, the LG scales unfavorably with L_{max} and favorably with N_r. Oppositely, the VG scales favorably with L_{max} and unfavorably with N_r.

This point is also clearly demonstrated in Fig. 5. Here we show the phase of the fifth harmonic calculated as the phase of the Fourier transform of the dipole velocity for 800 nm and a peak intensity of 1.138×10^{14} W/cm^2. In panel (a), we study the convergence of the phase as a function of L_{max} for a fixed number of grid points, $N_r = 1600$ in the LG and 1800 in the VG, and in panel (b), we study the convergence with respect to N_r for a fixed $L_{max} = 35$ in the LG and 15 in the VG. We see that the results are more sensitive to variations in L_{max} than in N_r and that the VG calculations converge faster. We have checked that the phases corresponding to the dipole and the acceleration forms transform as implied by Eq. (2). We now turn to a more detailed discussion of this latter point. Although the spectra of the three forms can be related to each other by Eq. (3) under the condition that $\langle \boldsymbol{r}(t_f) \rangle \approx \langle \dot{\boldsymbol{r}}(t_f) \rangle \approx 0$,

TABLE I. The phases P_ζ in radians of the three forms for the fifth harmonic, obtained by Fourier transform (FT) of the time-dependent expectation values, the reduced form Eq. (19), and full form Eq. (2), respectively, for a laser wavelength of 800 nm and an intensity of 0.3×10^{14} W/cm^2. P_z ($P_{\dot{z}}$) obtained by FT is used as a reference value to obtained $P_{\dot{z}}$ ($P_{\ddot{z}}$) by Eq. (19) and Eq. (2), respectively.

Gauge	Method	P_z	$P_{\dot{z}}$	$P_{\ddot{z}}$
	FT	−1.240 684	0.338 6080	1.874 558
Length	Reduced form		0.330 1123	1.909 404
	Full form		0.338 6096	1.874 555
	FT	−1.241 104	0.339 7798	1.873 470
Velocity	Reduced form		0.329 6923	1.910 576
	Full form		0.337 7585	1.876 662

the phases of the Fourier transforms of the three forms generally have to be related by Eq. (2). If it happens that $\langle \boldsymbol{r}(t_f) \rangle = \langle \dot{\boldsymbol{r}}(t_f) \rangle = 0$, Eq. (2) reduces to

$$\int_0^{t_f} \langle \dot{\boldsymbol{r}} \rangle e^{-i\omega t} dt = i\omega \int_0^{t_f} \langle \boldsymbol{r} \rangle e^{-i\omega t} dt,$$
$$\int_0^{t_f} \langle \ddot{\boldsymbol{r}} \rangle e^{-i\omega t} dt = i\omega \int_0^{t_f} \langle \dot{\boldsymbol{r}} \rangle e^{-i\omega t} dt. \tag{18}$$

Hence, in this case, the phase relationships have the simple forms

$$P_{\dot{\boldsymbol{r}}}(\omega) = \pi/2 + P_{\boldsymbol{r}}(\omega),$$
$$P_{\ddot{\boldsymbol{r}}}(\omega) = \pi/2 + P_{\dot{\boldsymbol{r}}}(\omega), \tag{19}$$

where the phases P_ζ ($\boldsymbol{\zeta} = \{\boldsymbol{r}, \dot{\boldsymbol{r}}, \ddot{\boldsymbol{r}}\}$) are defined in the range of $(-\pi, \pi]$. The strict condition $\langle \boldsymbol{r}(t_f) \rangle = \langle \dot{\boldsymbol{r}}(t_f) \rangle = 0$ is however hard to achieve. Though the absolute values of $\langle \boldsymbol{r}(t_f) \rangle$ and $\langle \dot{\boldsymbol{r}}(t_f) \rangle$ are so small that the effects on the spectrum intensity can be neglected, the effects on the harmonic phases cannot be neglected. In Table I, the phases of the fifth harmonic obtained from the Fourier transforms of the three forms are shown and compared to the corresponding ones obtained by the simplified Eq. (19) and the ones obtained by the full relationship of Eq. (2). From Table I, it can be seen that even for the weak laser field with an intensity of 0.3×10^{14} W/cm^2, where the HHG spectra of the three forms relate simply to each other by Eq. (3) [see Fig. 2], the phases of the three forms obtained by Eq. (19) are different from the reference values obtained by the Fourier transform of the corresponding time-dependent expectation value. The phases obtained from Eq. (2) are in good agreement with the reference values. Thus, it can be concluded that the reduced form (3) can be used only to relate the spectra, while for the phases, the full relationship (2) should be used.

To address the question of computational efficiency in the length and velocity gauges, we performed calculations at various laser intensities. The calculation at each intensity was performed on two AMD/Opteron 2.6-GHz processors in parallel with 8 gigabytes of memory. Both the number of grid points and L_{max} influence the memory need and calculation time for the solution of the TDSE. The results are shown in Fig. 6, where the black-square curves show the behavior of
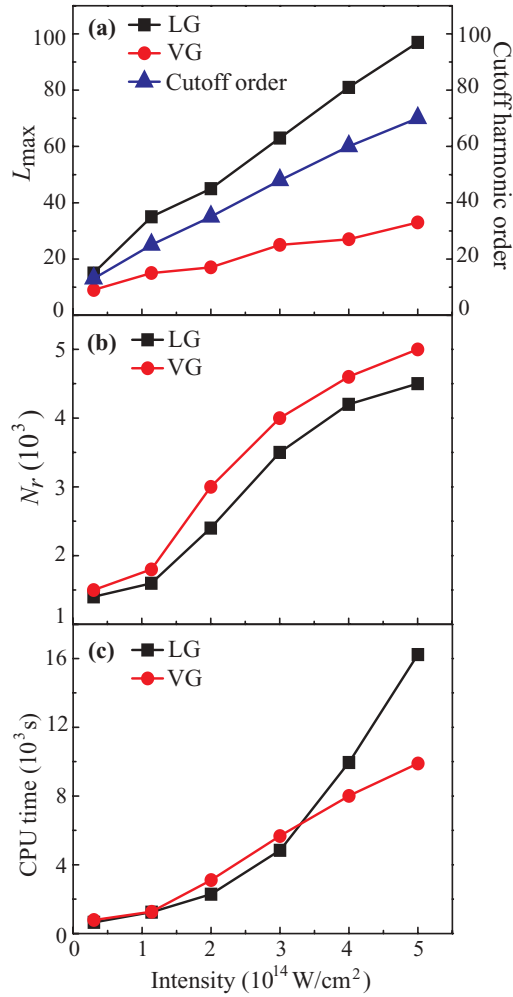
FIG. 6. (Color online) (a) Maximal number of angular momenta, L_{max}, in the expansion (9), (b) number of radial grid points, N_r, and (c) the total CPU time versus the increase in laser intensity. Black-square and red-circle curves refer to the calculation performed in the LG and the VG, respectively. The blue-triangle curve in (a) denotes the cutoff order versus the laser intensity. At the intensities $I = (0.3, 1.138, 2, 3, 4, 5) \times 10^{14}$ W/cm^2, the radial grid extends to 125, 125, 275, 425, 425, and 475 bohr, respectively.

the parameters used in the LG and the red-circle curves show the VG case. In Fig. 6(a), the blue-triangle curve denotes the cutoff order versus laser intensity following from the cutoff law $n = (3.17U_p + I_p)/\omega_0$ with U_p the ponderomotive potential and I_p the ionization potential [50]. We include the cutoff order for reasons discussed in the following. From Fig. 6(a), we see that each intensity L_{max} used in the LG is larger than the corresponding cutoff order, while L_{max} used in the VG is about half of the cutoff order. Moreover, with the increase of the laser intensity, the rate of increase of the slope for L_{max} versus intensity in the LG is much higher than that in the VG. In other words, along with the increase of laser intensity, L_{max} in the LG increases much faster than in the VG. In both gauges the comparison with the cutoff order is interesting, as can be simply seen in the photon picture: In principle, to represent the spectrum accurately up to the cutoff order n, one would expect it to be necessary to include at least $L_{max} = n$ angular

momenta, due to the dipole selection rule $l \to l \pm 1$ for each photon absorption. On the other hand, the fact that the final recombination step in the HHG process has to occur, in the present hydrogenic case, from a state of p ($l = 1$) symmetry, puts restrictions on the simple expectation and leads to the consideration of multiphoton absorption pathways leading to p states from which the recombination occurs. In such a line of reasoning the marked difference in the L_{max} scaling in Fig. 6(a) is a demonstration of the population of high L values occurring in the LG during the pulse.

In Fig. 6(b), we plot the number of grid points (N_r) versus the laser intensity. It is seen that, although we need more grid points in the VG than in the LG, the slopes of the two lines are quite similar. The number of grid points required in the VG is always about ∼500 larger than that required in the LG. That is to say, with the increase of the laser intensity, the combination of grid points and angular basis in the LG will be larger than that in VG, and hence larger memory and longer computation time will be spent in the LG case compared to the VG case. In Fig. 6(c), we compare the CPU time spent at different laser intensities in LG and VG calculations. It can be seen that the CPU time in the VG increases linearly with the laser intensity, while in the LG the slope of the curve increases with the laser intensity. Below an intensity of 3.25×10^{14} W/cm^2, the cost in CPU time in the two gauges is comparable. At higher intensity, however, the calculation in the VG will save much time. For a laser intensity equal to 5×10^{14} W/cm^2, the calculation in the VG is almost twice as fast as that in the LG.

IV. CONCLUSIONS

In this paper, we calculated the high-order harmonic spectra of the hydrogen atom in three forms (the dipole, dipole velocity, and acceleration forms) based on two gauges (the length and velocity gauges) by numerically solving the TDSE. Both the length and velocity gauges give almost identical results. However, the calculations in the two gauges require different kinds of parameters to converge. As was shown by the results of calculations and as expected on physical grounds (see Sec. III), one has to use a larger angular basis (L_{max}) in the length gauge and more grid points (N_r) in the velocity gauge. Moreover, the increase of the laser intensity, L_{max}, is faster in the length gauge than in the velocity gauge, while N_r increases at comparable speeds in the two gauges. As a result, at high laser intensity, the calculation in the velocity gauge is more efficient than that in the length gauge. It is also worth noting that, in this paper, we considered the case of the hydrogen atom in a linear polarized laser field, in which case the azimuthal magnetic quantum number m is fixed to zero. This means that there is no dependence on the azimuthal angle, ϕ, rendering the problem two dimensional with the angular part expanded by $\sum_{l=0}^{L_{max}} 1 = (L_{max} + 1)$ terms of spherical harmonic $\{Y_{l0}\}$ functions. Nevertheless, when aligned and oriented molecules are considered or a laser field with a polarization different from linear is used, the problem becomes three dimensional and m varies from $-l$ to l with l ranging from 0 to L_{max}, as used in Eq. (9), and hence the angular part is described by $\sum_{l=0}^{L_{max}} (2l + 1) = (L_{max} + 1)^2$ terms of spherical harmonics $\{Y_{lm}\}$. Thus, with the increase of laser intensity, the number of the terms of $\{Y_{lm}\}$ describing the angular part

increases at a speed of $(L_{max} + 1)^2$. It can be expected that, in three-dimensional cases, the efficiency of calculations in the VG will become more striking.

In addition to the benchmark data obtained from these convergence studies, in this paper we have stressed the importance of using the kinematical momenta $\boldsymbol{\pi} = \boldsymbol{p} + \boldsymbol{A}(t)$ when calculating the dipole velocity expectation value in the velocity gauge, and in particular we have addressed the question of how the phases of the harmonics are related in different gauges. Understanding the phase relationship of harmonics across forms and gauges is important in the upcoming discussion of how to produce harmonics with nonlinear polarization [28–30].

[1] P. B. Corkum, Phys. Rev. Lett. **71**, 1994 (1993).

[2] T. Brabec and F. Krausz, Rev. Mod. Phys. **72**, 545 (2000).

[3] C. Winterfeldt, C. Spielmann, and G. Gerber, Rev. Mod. Phys. **80**, 117 (2008).

[4] P. Agostini and L. F. DiMauro, Rep. Prog. Phys. **67**, 813 (2004).

[5] G. Sansone *et al.*, Science **314**, 443 (2006).

[6] J. J. Carrera, X. M. Tong, and Shih-I Chu, Phys. Rev. A **74**, 023404 (2006).

[7] E. Goulielmakis, V. S. Yakovlev, A. L. Cavalieri, M. Uiberacker, V. Pervak, A. Apolonski, R. Kienberger, U. Kleineberg, and F. Krausz, Science **317**, 769 (2007).

[8] M. Lein, N. Hay, R. Velotta, J. P. Marangos, and P. L. Knight, Phys. Rev. A **66**, 023805 (2002).

[9] T. Kanai, S. Minemoto, and H. Sakai, Nature (London) **435**, 470 (2005).

[10] C. Vozzi *et al.*, Phys. Rev. Lett. **95**, 153902 (2005).

[11] C. B. Madsen and L. B. Madsen, Phys. Rev. A **76**, 043419 (2007).

[12] X. Zhou, R. Lock, W. Li, N. Wagner, M. M. Murnane, and H. C. Kapteyn, Phys. Rev. Lett. **100**, 073902 (2008).

[13] O. Smirnova, Y. Mairesse, S. Patchkovskii, N. Dudovich, D. Villeneuve, P. Corkum, and M. Y. Ivanov, Nature (London) **460**, 972 (2009).

[14] A. D. Bandrauk, S. Chelkowski, D. J. Diestler, J. Manz, and K.-J. Yuan, Phys. Rev. A **79**, 023403 (2009), and references therein.

[15] C. Leone, S. Bivona, R. Burlon, F. Morales, and G. Ferrante, Phys. Rev. A **40**, 1828 (1989).

[16] T. K. Kjeldsen and L. B. Madsen, J. Phys. B **37**, 2033 (2004).

[17] Y. J. Chen and B. Hu, Phys. Rev. A **80**, 033408 (2009).

[18] L. B. Madsen and D. Dimitrovski, Phys. Rev. A **78**, 023403 (2008).

[19] R. M. Potvliege and R. Shakeshaft, in *Atoms in Intense Laser Fields*, edited by M. Gavrila (Academic, New York, 1992), pp. 337–433.

[20] N. Ben-Tal, N. Moiseyev, and R. Kosloff, Phys. Rev. A **48**, 2437 (1993).

[21] N. Moiseyev, M. Chrysos, O. Atabek, and R. Lefebvre, J. Phys. B **28**, 2007 (1995).

[22] M. Plummer and C. J. Nobel, J. Phys. B **35**, L51 (2002).

[23] P. Zdanska, V. Averbukh, and N. Moiseyev, J. Chem. Phys. **118**, 8726 (2003).

[24] O. E. Alon, V. Averbukh, and N. Moiseyev, Adv. Quant. Chem. **47**, 393 (2004).

[25] F. H. M. Faisal, J. Z. Kaminski, and E. Saczuk, Phys. Rev. A **72**, 023412 (2005).

[26] E. Mese and R. M. Potvliege, J. Phys. B **39**, 431 (2006).

[27] E. Cormier and P. Lambropoulos, J. Phys. B **29**, 1667 (1996).

[28] X. Zhou, R. Lock, N. Wagner, W. Li, H. C. Kapteyn, and M. M. Murnane, Phys. Rev. Lett. **102**, 073902 (2009).

[29] A. Etches, C. B. Madsen, and L. B. Madsen, Phys. Rev. A **81**, 013409 (2010).

[30] S. Ramakrishna, P. A. J. Sherratt, A. D. Dutoi, and T. Seideman, Phys. Rev. A **81**, R021802 (2010).

[31] G. L. Kamta and A. D. Bandrauk, Phys. Rev. A **71**, 053407 (2005).

[32] M. Lein, N. Hay, R. Velotta, J. P. Marangos, and P. L. Knight, Phys. Rev. Lett. **88**, 183903 (2002).

[33] D. A. Telnov and S.-I. Chu, Phys. Rev. A **71**, 013408 (2005).

[34] F. He, C. Ruiz, and A. Becker, Phys. Rev. A **75**, 053407 (2007).

[35] A.-T. Le, R. Della Picca, P. D. Fainstein, D. A. Telnov, M. Lein, and C. D. Lin, J. Phys. B **41**, 081002 (2008).

[36] I. A. Ivanov and A. S. Kheifets, Phys. Rev. A **79**, 053827 (2009).

[37] E. Lorin, S. Chelkowski, and A. D. Bandrauk, New J. Phys. **10**, 025033 (2008).

[38] E. Lorin, S. Chelkowski, and A. Bandrauk, Comput. Phys. Commun. **177**, 908 (2007).

[39] M. B. Gaarde, J. L. Tate, and K. J. Schafer, J. Phys. B **41**, 132001 (2008).

[40] C. B. Madsen and L. B. Madsen, Phys. Rev. A **74**, 023403 (2006).

[41] C. B. Madsen, A. S. Mouritzen, T. K. Kjeldsen, and L. B. Madsen, Phys. Rev. A **76**, 035401 (2007).

[42] U. Peskin, O. E. Alon, and N. Moiseyev, J. Chem. Phys. **100**, 7310 (1994).

[43] T. K. Kjeldsen, L. A. A. Nikolopoulos, and L. B. Madsen, Phys. Rev. A **75**, 063427 (2007).

[44] T. K. Kjeldsen, Ph.D. thesis, Aarhus University, 2007 [http://www.phys.au.dk/main/publications/PhD/Thomas_Kim_Kjeldsen.pdf].

[45] M. O. Scully and M. Suhail Zubairy, *Quantum Optics* (Cambridge University Press, Cambridge, 1997).

[46] L. B. Madsen, Phys. Rev. A **65**, 053417 (2002).

[47] F. H. M. Faisal, J. Phys. B **40**, F145 (2007).

[48] H. G. Müller, Laser Phys. **9**, 138 (1999).

[49] H. A. Bethe and E. E. Salpeter, *Quantum Mechanics of One- and Two-electron Atoms* (Springer, Berlin, 1957).

[50] M. Lewenstein, P. Balcou, M. Y. Ivanov, A. L'Huillier, and P. B. Corkum, Phys. Rev. A **49**, 2117 (1994).